DOI: 10.1088/2632-959X/ac0596

PEG size effect and its interaction with Fe_3O_4 nanoparticles synthesized by solvothermal method: morphology and effect of pH on the stability

To cite this article: Eliane A Namikuchi *et al* 2021 *Nano Ex.* **2** 020022

NANO EXPRESS

PAPER

PEG size effect and its interaction with Fe_3O_4 nanoparticles synthesized by solvothermal method: morphology and effect of pH on the stability

Eliane A Namikuchi[1], **Rafael D L Gaspar**[1], **Douglas S da Silva**[1], **Ivo M Raimundo Jr**[1,*] **and Italo O Mazali**[2,*]

[1] Institute of Chemistry, PO Box 6154, University of Campinas-UNICAMP, 13083-970, Campinas, SP, Brazil
[2] Laboratory of Functional Materials, Institute of Chemistry, PO Box 6154, University of Campinas-UNICAMP, 13083-970, Campinas, SP, Brazil
* Authors to whom any correspondence should be addressed.

E-mail: mazali@unicamp.br **and** ivo@unicamp.br

OPEN ACCESS

RECEIVED
16 December 2020

REVISED
16 April 2021

ACCEPTED FOR PUBLICATION
26 May 2021

PUBLISHED
4 June 2021

Keywords: magnetic nanoparticles, iron oxide, magnetite, PEG, solvothermal method

Supplementary material for this article is available online

Abstract

The synthesis and characterization of Fe_3O_4 magnetic nanoparticles (MNPs) obtained by the solvothermal method in ethyleneglycol with the addition of polyethyleneglycol (PEG) with molar mass of 4000, 8000 and 20000 g mol^{-1} are described, aimed at evaluating its effect on the size, morphology and stability of the nanoparticle. The syntheses were carried out by solubilizing the precursors at 85 and 140 °C, providing smaller nanoparticles as well as smaller crystallites at higher temperatures, while the effect of PEG was less evident. Measurements of nanoparticle surface areas synthesized with PEG 4000 and 20000 g mol^{-1} at 140 °C provided values of 76 and 14 m^2 g^{-1}, respectively, indicating that PEG 4000 surrounds the crystallites, while PEG 20000 preferably surrounds the whole MNP. As a consequence, MNP with very dissimilar porosities were obtained. Electron energy loss spectroscopy (EELS) indicated that MNP synthesized with PEG 20000 possesses higher electronic density than those obtained with PEG 4000, in agreement with the surface area results. Infrared spectroscopy and thermogravimetric analysis demonstrated the presence of PEG in the particles, whose amount increased as the particle size decreased. Dynamic Light Scattering (DLS) measurements showed that MNP hydrodynamic radius increases with the PEG size and stability in solution increases from pH 5.0 to 9.0 for smaller NP, while polymer presents slight effect on stability for the larger particles. The results obtained in this work show that properties of MNP can be tuned by the dissolution temperature of the chemical precursors and the PEG molar mass, changing their porosity and stability in solution, that are important variables in processes of adsorption, drug delivery and sensor developing.

1. Introduction

Since the discovery of the magnetic properties and biocompatibility of magnetic nanoparticles (MNPs), those constituted of iron oxides have shown significant uses in biomedical applications [1, 2], mainly in processes of magnetic resonance imaging [3, 4], drug delivery [5] and cancer treatment by hyperthermia [6, 7]. In addition, the magnetic properties of these nanoparticles have facilitated processes of separation, allowing the detection of metal ions [8–10] and removal of pollutants [11–13] in different media.

MNPs of iron oxide can be obtained by different methods, such as co-precipitation [14], thermal decomposition [15], microemulsion [16], sonochemical [17], solvothermal [18], among others. The preparation method is fundamental to determine the characteristics of MNPs, such as morphology and size distribution. Co-precipitation is the most used method to prepare iron oxide MNPs, due to its simplicity and low cost. This

method produces crystallites with average size around 10 nm, and, when synthesized with the addition of polyphosphate [19] and mannitol [20], respectively, they present improvement in colloidal stability, resistance to the presence of proteins and, even so, strong responsiveness to the magnetic field. Other surfactants as oleic acid, sodium citrate and Triton X-100 [21] also have been used. Besides bringing great advantages concerning the dispersion of MNPs [22], oleic acid and trisodium citrate can also allow better control of hyperthermia temperature treatment [23]. The MNPs with dimensions around 10–20 nm present better performance as they exhibit superparamagnetic behavior, which allow them to rapidly respond to an external magnetic field, with remanence and coercitivity of low magnitudes [24]. The MNPs with dimensions $>$20 nm can present an enhancement in the magnetic saturation; however, the transition from superparamagnetic to ferromagnetic behaviors will be also induced [25].

Crystallites of iron oxide with dimensions $<$20 nm can form clusters, resulting in secondary structures, which present magnetic saturation values much more intense, because each crystallite is able to maintain its superparamagnetic behavior [26]. Due to this characteristic, clusters of crystallites with different dimensions have been explored for several applications, mainly for the development of SERS substrates [27], processes of catalysis [28] and bioseparation [26]. These secondary structures, constituted by several crystallites, can be achieved by the solvothermal method, which has the advantage of providing monodisperse and hydrophilic nanoparticles with a degree of homogeneity higher than those provided by other methods [25, 26]. Dong *et al* [29] synthesized Fe_3O_4 MNPs with high porosity, high surface area and strong magnetic response. The nanoparticles were synthesized from $FeCl_3{\cdot}6H_2O$ by the solvothermal method, using ammonium acetate and sodium citrate in ethyleneglycol. Ammonium acetate acted as a porogenic agent, source of alkali and reducing reagent, in conjunction with ethyleneglycol, while sodium citrate acted as MNP stabilizer and modifier [29]. The effect of sodium citrate was investigated, producing smaller crystallites and MNPs with higher surface area when higher concentration was employed. The amount of ammonium acetate also affected the surface area of the nanoparticle, which increased as the concentration of the reagent increased, reaching a maximum, and then decreasing with further increasing of reagent concentration. This result is supposedly related to the pH of the medium, which increased according to ammonium acetate amount, therefore increasing the reaction rate, producing denser clusters. The nature of electrostatic stabilizer also affected MNP and crystallite sizes. Kim *et al* [30] verified the effect of sodium citrate, poly-ethyleneglycol (PEG 8000) and didodecyldimethylammonium bromide (DMAB), respectively, on the solvothermal synthesis of Fe_3O_4 MNPs in ethyleneglycol, using sodium acetate as stabilizer to avoid agglomeration of primary particles. Nanoparticles with sizes ranging from 174 to 336 nm and constituted of crystallites ranging from 11.6 to 21.3 nm were obtained, including those from the synthesis without the addition of stabilizer. Interestingly, the use of sodium citrate provided the largest particles with smallest crystallites, while DMAB produced the smallest particle size and narrowest size distribution. In addition, nanoparticles presented good dispersibility in water. The addition of 4-poly(vinylpyridine) in the synthesis of Fe_3O_4 in sodium acetate/ethyleneglycol solution produced mesoporous nanoparticles, with size of 240 nm and crystallites of 35.5 nm, able to remove Congo red from water, as described by Zeng *et al* [31]. According to the authors, 4-poly(vinylpyridine) can interact with the crystalline nuclei and reduce their growth during the hydrothermal reaction. In addition, this polymer can modify the surface of the crystalline nucleus, favoring the assembling of porous regular structures, with a uniform size distribution.

The stability of the magnetic nanoparticles dispersed in water is of great concern because agglomeration impairs their application in many areas, such as drug delivery, extraction and sensors. Agglomeration can occur due to the strong dipole-dipole interactions among the particles and to their high surface energies [32]. Therefore, surface modification of the nanoparticle is necessary in order to overcome this drawback, providing stabilization of MNP, which are mainly based on electrostatic (van der Waals and double layer), steric (polymeric, surfactant) and electrosteric forces [32]. Polymers, such as polyvinylalcohol (PVA), polyacrylic acid, polyethyleneimine (PEI), dextran, polyethyleneglycol (PEG) and surfactants, such as cetyltrimethylammonium bromide (CTAB), are usual modifiers to improve the stability of MNP. PEG, being biocompatible and hydrophilic, is often used as modifier/stabilizer of MNPs [32]. Despite its favorable characteristics, the modification of MNP with PEG is not straightforward, being usually performed after the synthesis of the nanoparticles and usually accomplished either by incorporating an appropriate functional group in the MNP or in the polymer [32]. The use of 3-aminopropyltrimethoxysilane (APTES) [33] has been described to modify the nanoparticles before PEGylation, while trimethoxysilanePEG [34] and dicarboxyl-terminated [35] have been used for modification of MNP. In spite of the strategies above mentioned, surface modification has been also made with as-prepared MNP and regular PEG [36].

The solvothermal method for preparation of MNP from iron(III) chloride frequently employs ethyleneglycol as a solvent, which also acts as reducing agent, and a precipitating agent, such as sodium acetate. Stabilizers are also added to the reaction medium to avoid particles agglomeration, as mentioned above. Polyethyleneglycol is used in the synthesis of iron oxide MNP as a stabilizer and polymers with different molar masses such as 8000 [30], 4000 [37] and 2000 g mol^{-1} [38] have been used. However, to the best of our

knowledge, there is no systematic study on the effect of PEG size on MNPs morphology and its stability in different pH values. Therefore, this work encompasses the synthesis of iron oxide MNP using ethyleneglycol as a solvent, in the presence of PEG with molar masses of 4000, 8000 and 20000 g mol^{-1}, evaluating their effect on the size, morphology and stability of the particles. In addition, syntheses were performed in two different temperatures (85 and 140 °C), as this variable also affects the size of the nanoparticles [37].

2. Experimental

2.1. Reagents

All reagents were used as received without further purification. Anhydrous iron(III) chloride ($FeCl_3$, MM = 162.20 g mol^{-1}), polyethyleneglycol (PEG) 8000 and 20000 (g mol^{-1}) were purchase from Sigma-Aldrich. Ethyleneglycol ($C_2H_4(OH)_2$, MM = 62.07 g mol^{-1}) and sodium acetate trihydrate ($NaAc{\cdot}3H_2O$, MM = 136.08 g mol^{-1}) were acquired from Synth. PEG 4000 (g mol^{-1}) was obtained from Vetec.

3. Synthesis of magnetic nanoparticles (MNPs)

A volume of 40 ml of ethyleneglycol was heated at a 140 °C in a 100-ml beaker. Afterwards, 8 mmol of $FeCl_3$ was added and the mixture was kept under stirring for 15 min after its temperature reaching again the temperature of 140 °C, thus making the salt soluble. Then, 1.0 g of PEG was added and, after stirring for 5 min, 26.5 mmol of $NaAc{\cdot}3H_2O$ were added, keeping the stirring for more 30 min. Finally, the solution was transferred to a PTFE-coated stainless steel autoclave (80 ml), which was placed in an oven at 200 °C for 8 h. After this period, the produced MNPs were separated from the solution with a magneto, washed with deionized water followed of ethanol and then dried in an oven at 60 °C for 8 h. This procedure was carried out using PEG 4000, PEG 8000 and PEG 20000, providing MNPs named 4K140, 8K140 and 20K140, respectively. Similar syntheses were performed at solubilization temperature of 85 °C, producing MNPs named 4K85, 8K85 and 20K85, respectively.

4. Characterization

4.1. X ray powder diffraction (XRD)

Measurements were performed at room temperature with a Shimadzu XRD-7000 diffractometer, running with CuKα radiation (λ = 1.5408 Å, 40 kV and 30 mA), within the interval from 5° to 70° (2θ), at 2° min^{-1}. The crystallite size (D) was calculated based on the most intense peak (311), employing the Scherrer equation ($D = k.\lambda/\beta.\cos\theta$) [39], where k is shape constant (k = 0.9 for spherical crystallite), λ is the x-ray wavelength (1.5408 Å), θ is the Brag diffraction angle (in grade) and β is the full-width at half-maximum (rad).

4.2. Transmission Electron Microscopy (TEM)

Morphology, and particle and crystallite sizes were evaluated with a Carl Zeiss microscope, model Libra 120 equipped with an omega 'Ω' filter *in-column*, operating at 80 or 120 kV, depending on the analysis conditions for obtaining optimized images. The samples were suspended in water, dripped on a copper grid (Ultrathin carbon film on lacey carbon support grid, 400 mesh, copper) and dried at room temperature. Electron Energy Loss Spectroscopy analysis were recorded for all spectra using fixed experimental conditions such as i) objective aperture of 90 μm resulting in a collection semi-angle around 15 mrad, ii) fixed spectrometer entrance aperture preserving same sample area size and iii) same dispersion magnification on spectrometer and on the digital recording system. Evaluation of a relative thickness (t/λ_{Ine}) was done using Log-Ratio method [40]. Olympus Cantega G2 (2048 × 2048 pixels) camera and iTEM software were used to register the images and spectra.

4.3. Analysis of the surface area and determination of pore size and volume

The nitrogen adsorption/desorption measurements were performed in a surface area and pore size analyzer ASAP 2020 Micromeritics. Samples were heated at 120 °C for 12 h before analysis. From these results, it was possible to determine the surface area using the BET method (Brunauer-Emmett-Teller). The pore diameter and volume were calculated using the Barrett-Joyner-Halenda (BJH) method.

4.4. Fourier transform infrared (FT-IR)

Measurements in the transmission mode were performed in KBr pellets at ambient temperature with an Agilent Cary 630 spectrometer. Spectra were acquired in the region from 400 to 4000 cm^{-1} as an average of 64 runs, with resolution of 4 cm^{-1}.

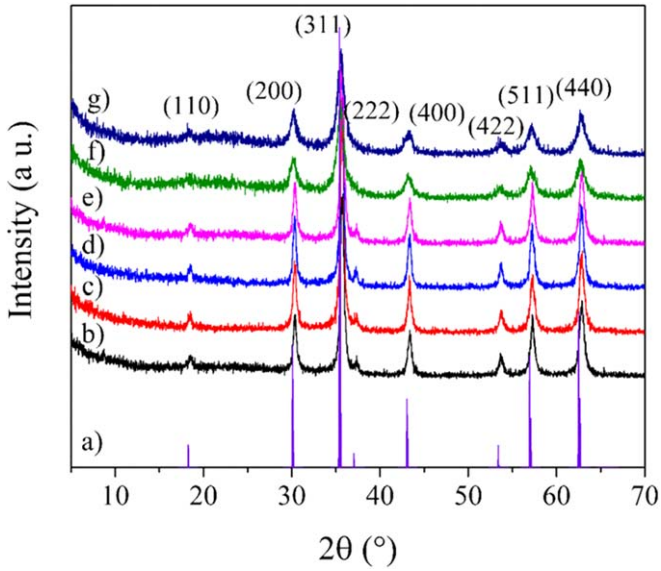

Figure 1. XRD pattern of the Fe_3O_4 JCPDS 19-0629 (a) and XRD of the Fe_3O_4 MNPs synthesized with PEG of different molar mass (4000, 8000 and 20000 g mol^{-1}) and with precursors solubilized at 85 °C: 4K85 (b), 8K85 (c), 20K85 (d) and 140 °C: 4K140 (e), 8K140 (f), 20K140 (g), respectively.

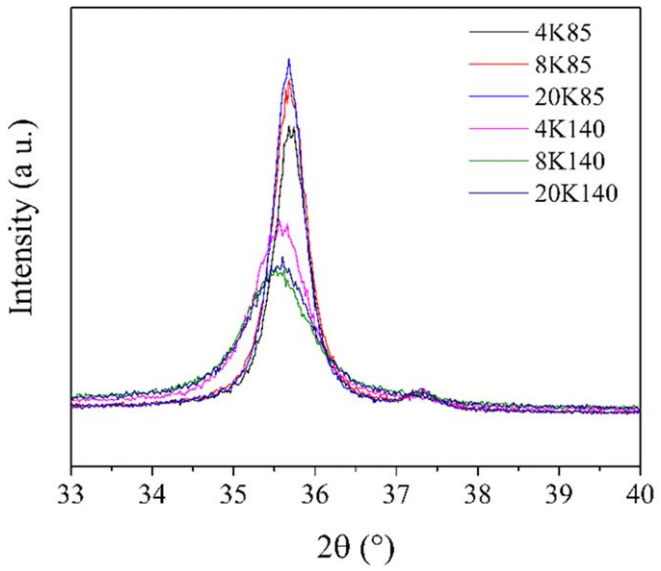

Figure 2. Detail of the diffraction peak (311) of the 85 °C and 140 °C of the Fe_3O_4 MNPs synthesized with PEG of different molar masses employed to calculate the crystallite size by Scherrer equation.

4.5. Thermogravimetric analysis (TGA)

A mass of 10–20 mg of sample was placed in a platinum crucible and analysis was performed with a TGA 2050 TA Instruments, at a heating rate of 10 °C min^{-1}, from 25 to 800 °C, in flowing argon atmosphere (100 ml min^{-1}).

4.6. Dynamic light scattering (DLS)

The particle sizes were measured with a Malvern equipment, model ZetasizerNano Zs-Zen3600. Samples (2.5 mg) were transferred to a 100-ml volumetric flask filled with deionized water and dispersed using at ultrasound bath for 25 min An aliquot of 2.5 ml of suspension was mixed with 2.5 ml of deionized water, acetate buffer (pH 5.0), phosphate buffer (pH 7.0) or carbonate buffer (pH 9.0) and 1.0 ml of this mixture was transferred to the measuring cell. The suspension was homogenized and measurements were performed during 1200 s, in intervals of 300 s.

Table 1. Crystallite sizes calculated for the Fe_3O_4 MNPs by Scherrer equation (see also table S1).

	Crystallite size (nm)		
Temperature (°C)	**4K**	**8K**	**20K**
85	17.2	16.8	18.9
140	10.6	8.4	8.7

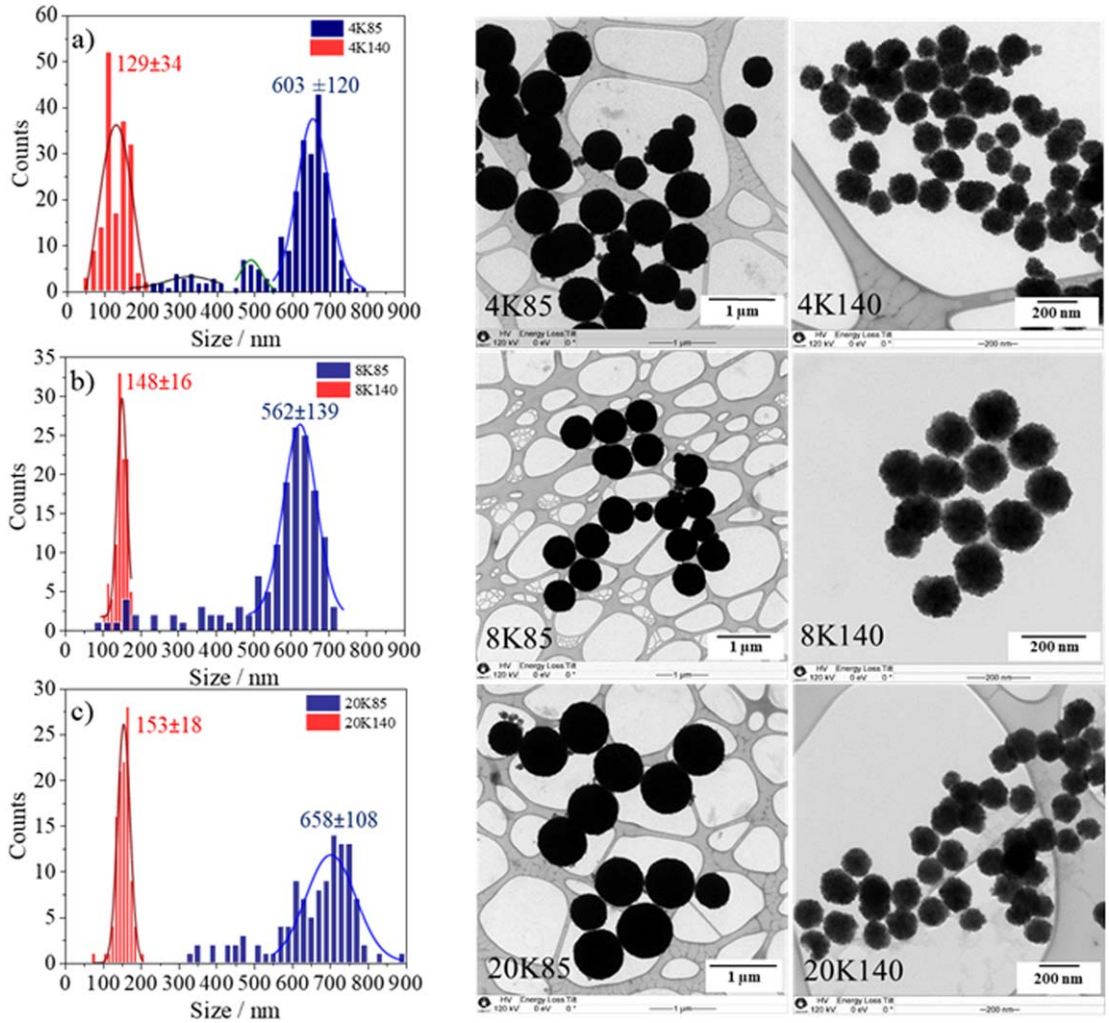

Figure 3. TEM images and respective size distribution histograms for 85 °C and 140 °C Fe_3O_4 MNPs: 4K85 and 4K140 (a), 8K85 and 8K140 (b) and 20K85 and 20K140 (c).

5. Results and discussion

Iron oxide nanoparticles can be obtained from several methods of synthesis. The solvothermal method is a versatile chemical route to prepare hydrophilic Fe_3O_4 MNPs, with a relatively narrow size distribution [25]. In addition, the temperature employed to solubilize the reagents allows obtaining MNPs with different sizes [37]. The MNPs obtained in the present study have similar size range of those described in a previous work, in which no significant variation in the magnetization values was observed [37]. The MNPs, whose precursors were solubilized at 85 and 140 °C and synthesized with PEG 4000, 8000 and 20000, were characterized by x ray diffraction and the effect of these variables on the particle size as well as on the crystallite size was evaluated. Figure 1 shows the x ray diffractograms of the MNPs, with diffraction lines indexed to the structure of the inverted spinel type according to magnetite catalog card JCPDS 19–629, suggesting that MNPs has a face-centered cubic structure.

In addition, it can be noted that increasing the dissolution temperature occurs a decrease in the relative intensities of the peaks. In order to verify this effect, the crystallite sizes were calculated by the Scherrer equation

Table 2. Values of (t/λ_{Ine}) obtained for 140 °C of five Fe_3O_4 MNPs.

PEG	MNP1	MNP2	MNP3	MNP4	MNP5	Mean	Standard deviation
4000	0.1642	0.1571	0.1528	0.1315	0.1594	0.15	0.01
8000	0.1125	0.1258	0.1241	0.1183	0.1308	0.122	0.006
20000	0.0975	0.1047	0.0923	0.0975	0.0793	0.094	0.008

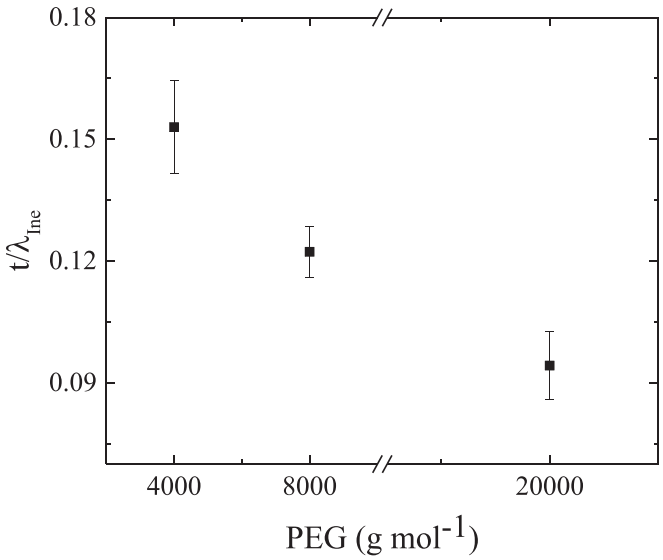

Figure 4. Effect of PEG polymeric chain size on the relative thickness (t/λ_{Ine}) of 4K140, 8K140 and 20K140 Fe_3O_4 MNPs of similar sizes.

[39], by employing the most intense diffraction line, attributed to the crystallographic plane (311), as highlighted in figure 2. Table 1 lists the values obtained in this calculation.

Electron diffraction and dark field images corroborate the analysis of the variation on grain size (see Supporting Information (available online at stacks.iop.org/NANOX/2/020022/mmedia), Figures S1 and S2 and table S1). Further electron diffraction confirms the high crystallinity degree of the crystallite obtained by solvothermal synthesis [41]. Therefore, the decrease of x ray peak intensity is associated to the decrease of the crystallite size. No significant effect was observed on the crystallite size when PEGs with different molar masses were used.

The reduction of the crystallite size as the dissolution temperature of precursors is decreased is associated to nucleation and growing steps. Higher temperatures increase the nucleation rate, favoring the formation of smaller crystallites (and also smaller NPs), while lower temperatures favor the growing step, producing higher crystallites, as described by Carvalho *et al* [37].

Observing the TEM images in figure 3, it can be noted the formation of nanostructured magnetic spheres produced by the solvothermal method, composed by several crystallites which aggregated to form larger secondary structures, therefore more stable than primary crystallites. In addition, size distribution is narrow for MNPs obtained from precursor dissolution performed at 140 °C and those obtained from dissolution at 85 °C seems to present a bimodal distribution. The formation of secondary structures from primary crystallites is also affected by the dissolution temperature and PEG plays an important role on the MNP porosity. PEG is supposed to surround the crystallites and its molar mass, and consequently its chain size, plays a fundamental role on the particle morphology and size distribution. For dissolution at 140 °C, the increase of PEG chain increases the particle average size and narrows its distribution (figures 3(a)–(c)), indicating the synergistic effect between PEG chain size and higher temperatures of precursors dissolution. Fine tuning of these parameters can allow size and distribution controls for several biomedical and sensing applications. Measurements of BET surface areas of 4K140 and 20K140 MNPs provided values of 76 and 14 $m^2\,g^{-1}$, respectively, indicating that PEG 4K surrounds the crystallites, while PEG 20K preferably surrounds the whole MNP, conducting to MNP with very dissimilar porosities. This assumption is also supported by the results obtained by BJH pore volume and pore diameter measurements, whose values are (0.22 $cm^3\,g^{-1}$ and 115 Å) and (0.12 $cm^3\,g^{-1}$ and 647 Å) for 4K140 and 20K140 MNPs, respectively. This result is important for the development of MNPs for removal of heavy metals, which requires porous particles in order to carry considerable amounts of these ions from aqueous systems [42, 43].

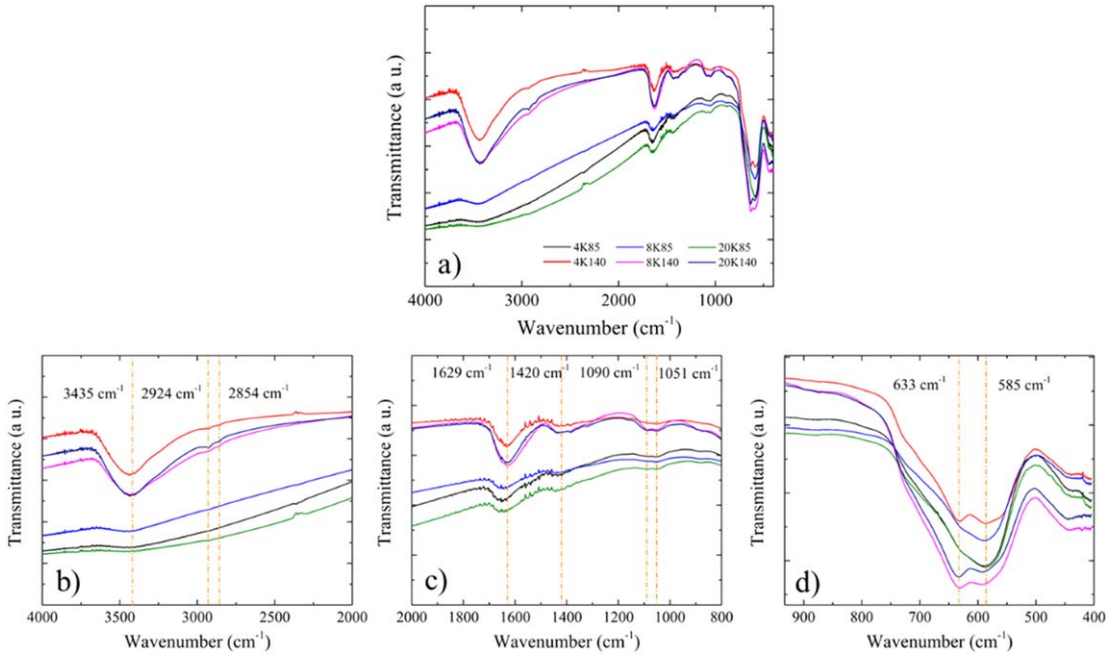

Figure 5. FT-IR absorption spectra of Fe_3O_4 MNPs obtained by using precursor dissolution temperature of 85 °C and 140 °C (a) and insets in the regions 4000–2000 cm^{-1} (b), 2000–800 cm^{-1}(c) and 900–400 cm^{-1} (d).

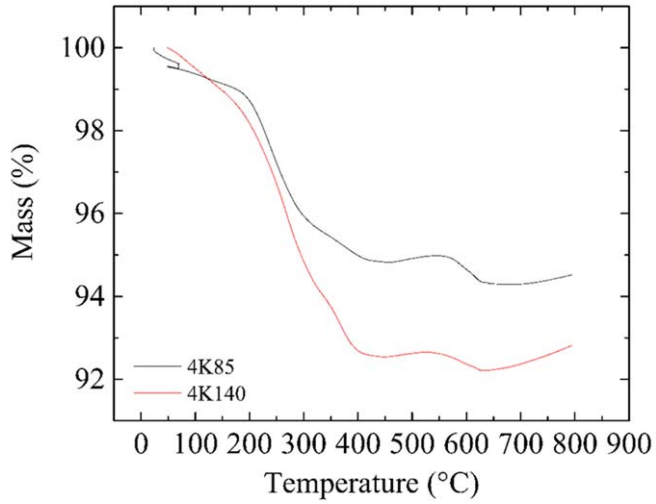

Figure 6. Termogravimetric curves of 4K85 and 4K140 Fe_3O_4 MNPs.

The effect of the PEG polymeric chain size on the electronic density of the NPs was also investigated by EELS, a characterization technique that does not require a specific crystalline structure, being able of analyzing materials with thicknesses from 15 to 500 nm [40]. Therefore, the effect of PEG on the morphology was investigated only for the MNPs smaller than 500 nm, that is, the 140°C MNPs, which have diameter around 160 nm. A set of five similar size MNPs prepared with each type of PEG was chosen for this study. Table 2 shows the relative thickness (t/λ_{Ine}) values obtained for each MNP, while figure 4 indicates a direct relationship between PEG molar mass and this parameter.

Since the size parameter is not varying, the decrease in (t/λ_{Ine}) as a function of the PEG chain reflects an increase in the mean free path as the PEG molar mass increases. It means that electronic density is proportional to the PEG molar mass, therefore indicating that denser MNPs are obtained with the use of PEG with higher molar mass, corroborating the results obtained by surface area measurements. Considering the experimental conditions, any difference in energy loss spectra and relative thickness parameter can be related to the electronic density (see Supporting Information). Thus, the more intense interaction, the higher is the electronic density in the sample, which means higher amount of iron in the particle and shorter the effective mean free path.

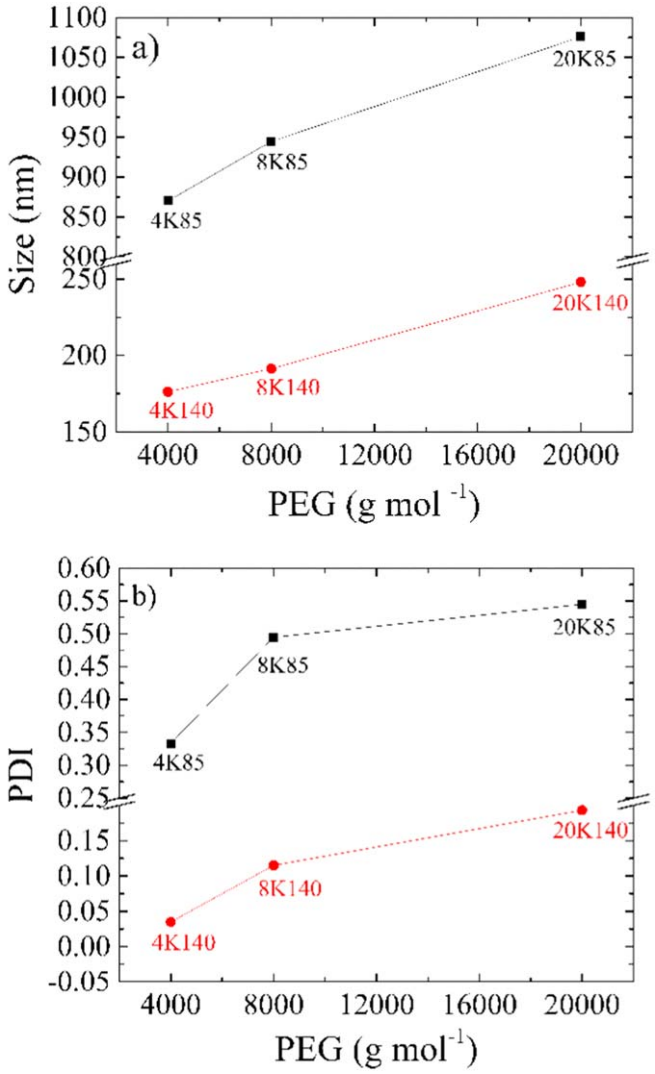

Figure 7. Size (a) and polydispersity index (b) of Fe_3O_4 MNPs synthesized as a function of PEG molar masses, with precursors dissolved at 85 and 140 °C (measurements in deionized water).

The MNPs were also analyzed by FT-IR spectroscopy, which provided information about the chemical groups on the particle surface, as shown in figure 5. It can be observed absorption bands around 3435 cm^{-1} and 1629 cm^{-1}, which are attributed to stretching [44] and bending [45] vibrations of the –O–H groups presented on the MNP surface, respectively. Low intensity absorption bands for MNPs obtained by using dissolution temperature of 140 °C are observed around 2924 cm^{-1} and 2854 cm^{-1}, which can be attributed to asymmetric and symmetric stretching vibrations of –C–H bonds [44, 46]. The absorption band centered at 1051 cm^{-1} can be attributed to stretching vibration of –C–C bond, while bands around 1420 cm^{-1} and 1090 cm^{-1} indicate stretching vibrations of –CO. These bands are more evident for the MNPs obtained when 140 °C was used for precursor dissolution, signalizing the PEG:Fe_3O_4 mass ratio is higher in these particles. Regarding the nanoparticles obtained from 85 °C, either these bands are not observed or they are weaker, probably because the larger size of the NPs that decreases the PEG:Fe_3O_4 mass ratio and causes a significant absorption of the radiation in the 4000–2000 cm^{-1} region. The absorption bands in the 700–400 cm^{-1} region appear in all spectra and can be ascribed to the Fe-O bond vibrations in the tetrahedral and octahedral sites [44, 47–49].

The PEG:Fe_3O_4 mass ratio was evaluated by thermogravimetric analysis, in inert atmosphere and temperature ranging from 25 to 800 °C. Figure 6 shows the thermogravimetric curves of nanoparticles synthesized in the presence of PEG 4000. The 140 °C MNPs present a higher mass loss than 85 °C MNPs, which are associated to the amount of polymer [50] and to the process of nanoparticle formation during the synthesis. The smaller nucleus formed at 140 °C can interact more effectively with PEG, therefore carrying a higher amount of polymer, results that corroborates those obtained by FT-IR spectroscopy. In addition, 140 °C MNPs have higher surface area, which can increase the PEG:Fe_3O_4 mass ratio for these samples. It can be noted that nanoparticles adsorb water efficiently via hydrogen bonds and decomposition of the polymer starts at a lower

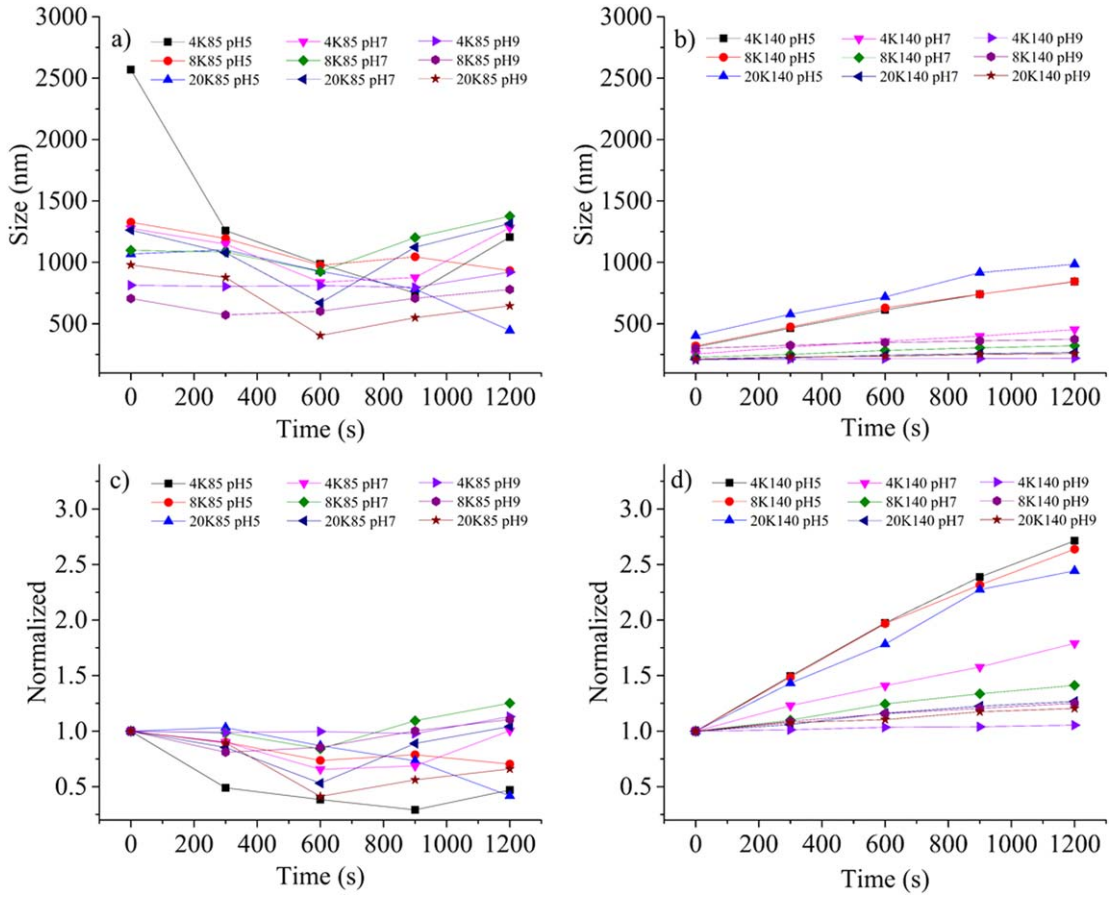

Figure 8. NP size as a function of time measured by DLS: 85 °C (a) and 140 °C (b) Fe_3O_4 MNPs measured particle size; 85 °C (c) and 140 °C (d) Fe_3O_4 MNPs normalized size taking the initial size as reference (original data in Tables S2 and S3 of Supplementary Information).

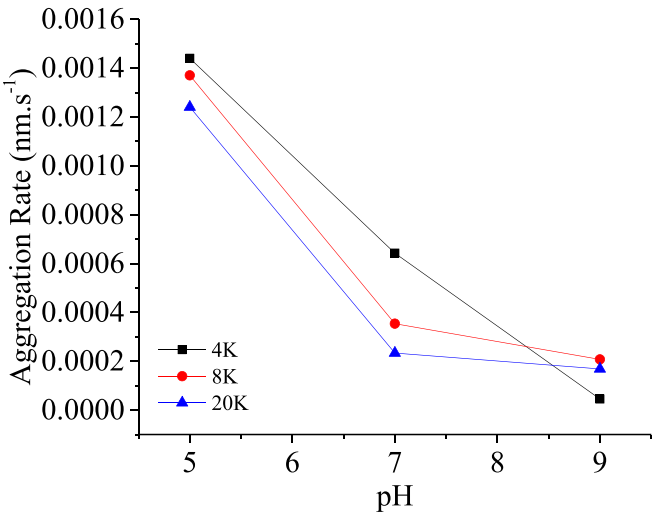

Figure 9. Effect of pH on the aggregation rates of 140 °C Fe_3O_4 MNPs.

temperature than the pure PEG, indicating a catalytic effect of the Fe_3O_4 MNPs [51]. Similar results were obtained for MNPs synthesized with PEG 8K and 20K (Figure S4 of Supporting Information).

The results obtained by FT-IR and TG confirm the presence of –OH groups of water molecules physio-sorbed on the MNP, which can provide hydrophilic character to them. In order to assess this stability, DLS measurements were performed in deionized water and buffer solutions at pH 5.0, 7.0 and 9.0. The suspensions of MNPs were prepared at the concentration of 25 mg L^{-1}, with the aid of ultrasound bath, in order to maintain

similar interactions between the particles, as they tend to aggregate and form clusters of different sizes [52]. Figure 7(a) shows the smaller size of the MNPs obtained with precursors dissolved at 140 °C compared to those obtained at 85 °C, while the hydrodynamic radius increases as a function of the molar mass of PEG, corroborating the result obtained by electronic density measurements that indicates that PEG 20K surrounds the MNP, while PEG 4K remains among the crystallites. In addition, a lower polydispersity is obtained when higher dissolution temperature is used, although it is also evident that increasing the PEG chain the polydispersity index increases, as shown in figure 7(b). The term 'polydispersity' (PDI or 'dispersity' as recommended by IUPAC) is used to describe the non-uniformity degree of the particle size distribution. Also known as heterogeneity index, PDI is a number calculated from a two-parameter fit to the correlation data (the cumulants analysis). This index is dimensionless and values smaller than 0.05 are mainly seen with highly monodisperse standards. PDI values higher than 0.7 indicate the sample has a very broad particle size distribution and is probably not suitable to be analyzed by the DLS technique. Different size distribution algorithms work with data that fit between these two extreme values of PDI (i.e., 0.05–0.7) [53]. Therefore, according to these values, it can be considered that 4K140 MNPs have a monodisperse distribution in suspension, while other MNPs present a population of low-to-medium polydispersity.

The stability of the MNPs in buffer solutions was evaluated by measuring their size increase as a function of time, demonstrating the aggregation rate. Buffer solution was added to MNP aqueous suspensions at the beginning of the measurements, therefore producing a change in pH as well as in the ionic strength of the medium. Figure 8 summarizes the results obtained, which also shows normalized values obtained by taking as reference the particle sizes at the beginning of the experiments ($t = 0$). Figure 8(a) shows that 85 °C NPs decrease in size at short times, presenting almost a random behavior as the measurement progresses. The size decrease can be explained by the effect of ionic strength that avoids the agglomeration of particles, whose size trend is summarized in figure 8(c). However, a more plausible reason concerns the sedimentation of the particles as a function of time due to their sizes, while the smaller ones remain in suspension. On the other hand, 140 °C MNPs undergo a significant effect of the solution pH, as shown in figures 8(b) and (d), in which particles increase their size almost three times at pH 5.0, due to agglomeration. Considering these results, it is clear that size of MNPs plays an important role on the stability, while the PEG chain size does not seem to affect it significantly in buffered solutions, as described for MNPs modified with PEG after their synthesis [54].

Figure 8(d) indicates that sizes of the 140 °C MNPs present virtually a linear behavior as a function of time, independently of the solution pH. This curve pattern is associated to the size of the MNPs as well as the surface characteristics, such as the presence of –OH groups from water molecules, that is practically absent on the surface of 85 °C NPs, as demonstrated by FT-IR. Thus, the aggregation rate for 140 °C NPs can be calculated as a function of time, as shown in figure 9. It can be noted that aggregation rate decreases as the solution pH increases, as in acidic pH MNPs are more susceptible to aggregate due to the neutralization of the negative charge on their surfaces. In addition, increasing the size of PEG chain, the stability of the MNPs are usually higher due to the steric hindrance, which keeps the particles apart from each other. It seems from figure 9 that steric hindrance plays an important role against aggregation for PEG 8K and 20K, as solution pH has little effect on the NPs stability above the value of 7.0. At pH 9.0, however, the 4K140 MNP, having a small amount of PEG on the surface, is highly charged, presenting the lowest aggregation rate. The polydispersity index of the MNPs obtained with precursors dissolution at 140 °C also present a small increase as a function of time, while those obtained from 85 °C vary significantly as shown in figure S5 (Supplementary Information). Therefore, 20K140 MNPs, followed of 8K140, seem to be useful for bioanalytical, clinic and medical applications, where the pH of fluids are between 7.0 and 8.0, as well as for the development of sensors for metal ions, that usually work in the 7 to 9 pH range.

6. Conclusion

Iron oxide NPs were synthesized by the solvothermal method in ethyleneglycol, by using PEG with molar masses of 4000, 8000 and 20000 g mol^{-1} and solubilizing the chemical precursors at 85 and 140 °C. Results obtained by TEM and BET showed that dissolution temperature of reagents affected the particle sizes and their distribution as well as the formation of respective aggregates. EELS showed that electronic density of particles synthesized by solubilizing the precursors at 140 °C increased as the PEG molar mass also increased, indicating PEG with high molar mass cover the NPs while it stands in between the crystallites when its molar mass is low. Infrared spectroscopy and thermogravimetric analysis demonstrated the presence of PEG in the particles, whose amount increased as the particle size decreased. DLS measurements showed that MNP hydrodynamic radius increase with the PEG size and stability in solution increases from pH 5.0 to 9.0 for smaller particles, while it presents slight effect on stability for larger ones. The results obtained in this work show MNPs morphological and dispersity properties can be tuned by the temperature of dissolution of the chemical precursors and the PEG

molar mass, allowing to vary their porosity and stability in suspension. These features enable the use of the synthesized MNPs for applications where controlled sorption processes are important variables, such as drug delivery, magnetic separation and sensor developing.

Acknowledgments

This is a contribution of INCTAA (CNPq 465768/2014-8 and FAPESP 2014/50951-4) and INOMAT - National Institute of Science and Technology in Complex Functional Materials (CNPq 465452/2014-0 and FAPESP 2014/50906-9). FAPESP (grants 2013/22127-2, 2014/50906-9) and CNPq (grant 407591/2016-8) are also acknowledged for the financial support. EAN (grant 141438/2016-9), IMRJ (grant 308424/2019-0) and IOM (grant 310131/2020-0) are thankful to CNPq for the fellowships. RDLG thanks FAPESP for the postdoctoral fellowship (grant 2018/20997-3).

Data availability statement

The data that support the findings of this study are available upon reasonable request from the authors.

ORCID iDs

Douglas S da Silva https://orcid.org/0000-0003-2212-8331
Ivo M Raimundo Jr https://orcid.org/0000-0002-5860-3133
Italo O Mazali https://orcid.org/0000-0001-5698-5273

References

[1] Cardoso V F, Francesko A, Ribeiro C, Bañobre-López M, Martins P and Lanceros-Mendez S 2018 Advances in magnetic nanoparticles for biomedical applications *Adv. Healthc. Mater.* **7** 1700845
[2] Hu Y, Mignani S, Majoral J-P, Shen M and Shi X 2018 Construction of iron oxide nanoparticle-based hybrid platforms for tumor imaging and therapy *Chem. Soc. Rev.* **47** 1874–900
[3] Lin Y-L, Lin Y-C, Wang L-J, Ngo S-T and Ma Y-H 2019 Renal perfusion assessment using magnetic nanoparticles with 7T dynamic susceptibility contrast MRI in rats *J. Magn. Magn. Mater.* **475** 76–82
[4] Han C, Zhang A, Kong Y, Yu N, Xie T, Dou B, Li K, Wang Y, Li J and Xu K 2019 Multifunctional iron oxide-carbon hybrid nanoparticles for targeted fluorescent/MR dual-modal imaging and detection of breast cancer cells *Anal. Chim. Acta* **1067** 115–28
[5] Moghadam N H, Salehzadeh S, Rakhtshah J, Moghadam A H, Tanzadehpanah H and Saidijam M 2019 Preparation of a highly stable drug carrier by efficient immobilization of human serum albumin (HSA) on drug-loaded magnetic iron oxide nanoparticles *Int. J. Biol. Macromol.* **125** 931–40
[6] Das P, Colombo M and Prosperi D 2019 Recent advances in magnetic fluid hyperthermia for cancer therapy *Colloid Surface B* **174** 42–55
[7] Kubovcikova M *et al* 2019 Poly-L-lysine designed magnetic nanoparticles for combined hyperthermia, magnetic resonance imaging and cancer cell detection *J. Magn. Magn. Mater.* **475** 316–26
[8] Mei M, Pang J, Huang X and Luo Q 2019 Magnetism-reinforced in-tube solid phase microextraction for the online determination of trace heavy metal ions in complex samples *Anal. Chim. Acta* **1090** 82–90
[9] Kim K T, Yoon S A, Ahn J, Choi Y, Lee M H, Jung J H and Park J 2017 Synthesis of fluorescent naphthalimide-functionalized Fe_3O_4 nanoparticles and their application for the selective detection of Zn^{2+} present in contaminated soil *Sensor Actuat. B-Chem.* **243** 1034–41
[10] De La Rosa-Romo L M, Oropeza-Guzmán M T, Olivas-Sarabia A and Pina-Luis G 2016 Flavone functionalized magnetic nanoparticles: a new fluorescent sensor for Cu^{2+} ions with nanomolar detection limit *Sensor Actuat. B-Chem.* **233** 459–68
[11] Tavakoli M, Hajimahmoodi M and Shemirani F 2014 Trace level monitoring of pesticides in water samples using fatty acid coated magnetic nanoparticles prior to GC-MS *Anal. Methods* **6** 2988–97
[12] Kumari M and Gupta S K 2018 Removal of aromatic and hydrophobic fractions of natural organic matter (NOM) using surfactant modified magnetic nanoadsorbents (MNPs) *Environ. Sci. Pollut. Res. Int.* **25** 25565–79
[13] Liu Z, Qi P, Wang J, Wang Z, Di S, Xu H, Zhao H, Wang Q, Wang X and Wang X 2020 Development, validation, comparison, and implementation of a highly efficient and effective method using magnetic solid-phase extraction with hydrophilic-lipophilic-balanced materials for LC-MS/MS analysis of pesticides in seawater *Sci. Total Environ.* **708** 135221
[14] Roth H-C, Schwaminger S P, Schindler M, Wagner F E and Berensmeier S 2015 Influencing factors in the co-precipitation process of superparamagnetic iron oxide nano particles: a model based study *J. Magn. Magn. Mater.* **377** 81–9
[15] Hufschmid R, Arami H, Ferguson R M, Gonzales M, Teeman E, Brush L N, Browning N D and Krishnan K M 2015 Synthesis of phase-pure and monodisperse iron oxide nanoparticles by thermal decomposition *Nanoscale* **7** 11142–54
[16] Scano A, Cabras V, Pilloni M and Ennas G 2019 Microemulsions: the renaissance of ferrite nanoparticle synthesis *J. Nanosci. Nanotechnol.* **19** 4824–38
[17] Vijayakumar R, Koltypin Y, Felner I and Gedanken A 2000 Sonochemical synthesis and characterization of pure nanometer-sized Fe_3O_4 particles *Mater. Sci. Eng. A* **286** 101–5
[18] Kim J *et al* 2018 Scalable solvothermal synthesis of superparamagnetic Fe_3O_4 nanoclusters for bioseparation and theragnostic probes *ACS Appl. Mater. Interfaces* **10** 41935–46

[19] Majeed J, Barick K C, Shetake N G, Pandey B N, Hassan P A and Tyagi A K 2015 Water-dispersible polyphosphate-grafted Fe_3O_4 nanomagnets for cancer therapy *RSC Adv.* **5** 86754–62

[20] Gawali S L, Barick B K, Barick K C and Hassan P A 2017 Effect of sugar alcohol on colloidal stabilization of magnetic nanoparticles for hyperthermia and drug delivery applications *J. Alloy Compd.* **725** 800–6

[21] Soares P I, Alves A M, Pereira L C, Coutinho J T, Ferreira I M, Novo C M and Borges J P 2014 Effects of surfactants on the magnetic properties of iron oxide colloids *J. Colloid Interface Sci.* **419** 46–51

[22] Soares P I, Laia C A, Carvalho A, Pereira L C, Coutinho J T, Ferreira I M, Novo C M and Borges J P 2016 Iron oxide nanoparticles stabilized with a bilayer of oleic acid for magnetic hyperthermia and MRI applications *Appl. Surf. Sci.* **383** 240–7

[23] Soares P I, Lochte F, Echeverria C, Pereira L C, Coutinho J T, Ferreira I M, Novo C M and Borges J P 2015 Thermal and magnetic properties of iron oxide colloids: influence of surfactants *Nanotechnology* **26** 425704

[24] Ganesan V, Louis C and Damodaran S P 2018 Novel nanofluids based on magnetite nanoclusters and investigation on their cluster size-dependent thermal conductivity *J. Phys. Chem. C* **122** 6918–29

[25] Lu A-H, Salabas E L and Schüth F 2007 Magnetic nanoparticles: synthesis, protection, functionalization, and application *Angew. Chem. Int. Ed.* **46** 1222–44

[26] Lu Z and Yin Y 2012 Colloidal nanoparticle clusters: functional materials by design *Chem. Soc. Rev.* **41** 6874–87

[27] Zou B, Niu C, Ma M, Zhao L and Wang Y 2019 Magnetic assembly route to construct reproducible and recyclable SERS substrate *Nanoscale Res. Lett.* **14** 369

[28] Li S, Liang W, Zheng F, Zhou H, Lin X and Cai J 2016 Lysine surface modified Fe_3O_4@SiO_2@TiO_2 microspheres-based preconcentration and photocatalysis for *in situ* selective determination of nanomolar dissolved organic and inorganic phosphorus in seawater *Sensor Actuat. B-Chem.* **224** 48–54

[29] Dong F, Guo W, Bae J-H, Kim S-H and Ha C-S 2011 Highly porous, water-soluble, superparamagnetic, and biocompatible magnetite nanocrystal clusters for targeted drug delivery *Chem. Eur. J.* **17** 12802–8

[30] Kim S, Katsumata K-I, Okada K and Matsushita N 2015 Highly dispersed iron oxide nanoparticles synthesized by solvothermal method adding electrostatic stabilizer *IEEE Trans. Magn.* **51** 5200304

[31] Zeng B, Yang L, Zheng W, Zhu J, Ma X, Liu X, Yuan C, Xu Y and Dai L 2018 Analysis of the formation process and performance of magnetic Fe_3O_4@Poly (4-vinylpyridine) absorbent prepared by *in situ* synthesis *J. Mater. Sci. Technol.* **34** 999–1007

[32] Ramimoghadam D, Bagheri S and Hamid S B A 2015 Stable monodisperse nanomagnetic colloidal suspensions: an overview *Colloid Surface B* **133** 388–411

[33] Hervé K *et al* 2008 The development of stable aqueous suspensions of PEGylated SPIONs for biomedical applications *Nanotechnology* **19** 465608

[34] Butterworth M D, Illum L and Davis S S 2001 Preparation of ultrafine silica- and PEG-coated magnetite particles *Colloids Surf. A Physicochem. Eng. Asp.* **179** 93–102

[35] Hu F Q, Wei L, Zhou Z, Ran Y L, Li Z and Gao M Y 2006 Preparation of biocompatible magnetic nanocrystals for *in vivo* magnetic resonance detection of cancer *Adv. Mater.* **18** 2553–6

[36] Mohanta S C, Saha A and Devi P S 2018 PEGylated iron oxide nanoparticles for pH responsive drug delivery application *Mater. Today-Proceedings* **5** 9715–25

[37] Da Costa Carvalho B, Andrade Corbi F C, Sigoli F A and Mazali I O 2016 Precursor dissolution temperature as a size-controller in Fe_3O_4 submicrospheres syntheses and their effect in the catalytic degradation of Rhodamine B *RSC Adv.* **6** 38617–23

[38] Huang Z, Wu K, Yu Q-H, Wang Y-Y, Xing J and Xia T-L 2016 Facile synthesis of size tunable Fe_3O_4 nanoparticles in bisolvent system *Chem. Phys. Lett.* **664** 219–25

[39] Patterson A L 1939 The Scherrer formula for x-ray particle size determination *Phys. Rev.* **56** 978

[40] Iakoubovskii K, Mitsuishi K, Nakayama Y and Furuya K 2008 Thickness measurements with electron energy loss spectroscopy *Microsc. Res. Tech.* **71** 626–31

[41] de Mello L B, Varanda L C, Sigoli F A and Mazali I O 2019 Co-precipitation synthesis of (Zn-Mn)-co-doped magnetite nanoparticles and their application in magnetic hyperthermia *J. Alloys Compd.* **779** 698–705

[42] Wang F-H, Jiang W, Fang Y and Cheng C-W 2015 Preparation of Fe_3O_4 magnetic porous microspheres (MPMs) and their application in treating mercury-containing wastewater from the polyvinyl chloride industry by calcium carbide method *Chem. Eng. J.* **259** 827–36

[43] Zhao J, Liu J, Li N, Wang W, Nan J, Zhao Z and Cui F 2016 Highly efficient removal of bivalent heavy metals from aqueous systems by magnetic porous Fe_3O_4-MnO_2: Adsorption behavior and process study *Chem. Eng. J.* **304** 737–46

[44] Hoa L T M, Dung T T, Danh T M, Duc N H and Chien D M 2009 Preparation and characterization of magnetic nanoparticles coated with polyethylene glycol *J. Phys. Conf. Ser.* **187** 012048

[45] Ai Z, Deng K, Wan Q, Zhang L and Lee S 2010 Facile microwave-assisted synthesis and magnetic and gas sensing properties of Fe_3O_4 nanoroses *J. Phys. Chem. C* **114** 6237–42

[46] Hu L, Hach D, Chaumont D, Brachais C-H and Couvercelle J-P 2008 One step grafting of monomethoxy poly (ethylene glycol) during synthesis of maghemite nanoparticles in aqueous medium *Colloids Surf. A Physicochem. Eng. Asp.* **330** 1–7

[47] Li P, Yu B and Wei X 2004 Synthesis and characterization of a high oil-absorbing magnetic composite material *J. Appl. Polym. Sci.* **93** 894–900

[48] Tie S-L, Lin Y-Q, Lee H-C, Bae Y-S and Lee C-H 2006 Amino acid-coated nano-sized magnetite particles prepared by two-step transformation *Colloids Surf. A Physicochem. Eng. Asp.* **273** 75–83

[49] Ma M, Zhang Y, Yu W, Shen H-y, Zhang H-q and Gu N 2003 Preparation and characterization of magnetite nanoparticles coated by amino silane *Colloids Surf. A Physicochem. Eng. Asp.* **212** 219–26

[50] Mukhopadhyay A, Joshi N, Chattopadhyay K and De G 2012 A facile synthesis of PEG-coated magnetite (Fe_3O_4) nanoparticles and their prevention of the reduction of cytochrome C *ACS Appl. Mater. Interfaces* **4** 142–9

[51] Durmus Z, Kavas H, Toprak M S, Baykal A, Altınçekiç T G, Aslan A, Bozkurt A and Coşgun S 2009 L-lysine coated iron oxide nanoparticles: synthesis, structural and conductivity characterization *J. Alloy Compd.* **484** 371–6

[52] Iyengar S J, Joy M, Ghosh C K, Dey S, Kotnala R K and Ghosh S 2014 Magnetic, x-ray and Mössbauer studies on magnetite/maghemite core-shell nanostructures fabricated through an aqueous route *RSC Adv.* **4** 64919–29

[53] Danaei M, Dehghankhold M, Ataei S, Hasanzadeh Davarani F, Javanmard R, Dokhani A, Khorasani S and Mozafari M R 2018 Impact of particle size and polydispersity index on the clinical applications of lipidic nanocarrier systems *Pharmaceutics* **10** 57

[54] Lim J K, Majetich S A and Tilton R D 2009 Stabilization of superparamagnetic iron oxide core-gold shell nanoparticles in high ionic strength media *Langmuir* **25** 13384–93